Journal of Magnetic Resonance 193 (2008) 199–206

Contents lists available at ScienceDirect

Journal of Magnetic Resonance

journal homepage: www.elsevier.com/locate/jmr

Spectrally resolved flow imaging of fluids inside a microfluidic chip with ultrahigh time resolution

Elad Harel *, Alex Pines

Materials Sciences Division, Lawrence Berkeley National Laboratory, and Department of Chemistry, University of California, Berkeley, CA 94720, USA

ARTICLE INFO

Article history:
Received 27 March 2008
Revised 25 April 2008
Available online 9 May 2008

Keywords:
Magnetic resonance
Imaging
Microfluidics
Lab-on-chip
Flow
Microcoil
Remote detection
Ultrahigh time resolution
Dispersion
Mixing
Chromatography

ABSTRACT

Microfluidics has advanced to become a complete lab-on-a-chip platform with applications across many disciplines of scientific research. While optical techniques are primarily used as modes of detection, magnetic resonance (MR) is emerging as a potentially powerful and complementary tool because of its non-invasive operation and analytical fidelity. Two prevailing limitations currently inhibit MR techniques on microfluidic devices: poor sensitivity and the relatively slow time scale of dynamics that can be probed. It is commonly assumed that the time scale of observation of one variable limits the certainty with which one can measure the complementary variable. For example, short observation times imply poor spectral resolution. In this article, we demonstrate a new methodology that overcomes this fundamental limit, allowing in principle for arbitrarily high temporal resolution with a sensitivity across the entire microfluidic device several orders of magnitude greater than is possible by direct MR measurement. The enhancement is evidenced by recording chemically resolved fluid mixing through a complex 3D microfluidic device at 500 frames per second, the highest recorded in a magnetic resonance imaging experiment. The key to this development is combining remote detection with a time 'slicing' of its spatially encoded counterpart. Remote detection circumvents the problem of insensitive direct MR detection on a microfluidic device where the direct sensitivity is less than 10^{-5} relative to traditional NMR, while the time slicing eliminates the constraints of the limited observation time by converting the time variable into a spatial variable through the use of magnetic field gradients. This method has implications for observing fast processes, such as fluid mixing, rapid binding, and certain classes of chemical reactions with sub millisecond time resolution and as a new modality for on-chip chromatography.

Published by Elsevier Inc.

1. Introduction

Lab-on-a-chip technologies, which enable the control of fluid flow on the micron and nano-scale, hold great promise for advancing research in a diversity of fields, ranging from ligand binding for drug development ([1]) to synthetic chemistry ([2]), as well as in performing fundamental studies of chemical, physical, and biological processes ([3]). Much effort has been devoted to understanding the fluid flow inside microfluidic devices since this plays a key role in their function ([4,5]). While optical methods exist for fluid tracing even at high velocities, they suffer from serious drawbacks such as a lack of chemically specificity and the need for optically transparent devices ([6]). Generally, one can either obtain a spectrum or an image but not both. Magnetic resonance imaging, on the other hand, is capable of routinely providing simultaneous spatial and spectral information, noninvasively and within opaque materials, through spectroscopic imaging ([7]). Doing so on a microfluidic chip is a formidable task due to the poor sensitivity of NMR, especially on channels with cross-sectional area less than 10^{-8} m^2. Compounding this problem is the fact that the radio-frequency (RF) excitation and detection must occur over the volume of the entire chip, while only a fraction is occupied by the fluid that gives rise to the NMR signal. For microfluidics the direct sensitivity is less than 10^{-5} of traditional high-resolution NMR under these conditions. While NMR surface coils can be used to increase sensitivity, they are, in general, limited to examining only a single or, at most, a very few number of points on the chip ([8]). Additionally, their large fingerprint (ca 1 mm) precludes examining regions of congested channels, common in sophisticated microfluidic devices. Although imaging gradients, could, in principle be used to differentiate channels that are close in space, this would negate to a large degree the advantages of using a small detector.

Remote detection ([9,10]) can overcome the limitations of direct MR imaging in cases where the sample is small relative to the detector by significantly increasing sensitivity. Additionally, it allows for the chemical-shift responsible for the NMR spectrum to be recovered outside the chip, a substantial advantage as local variations in the magnetic field due to susceptibility gradients at the fluid, glass, and air interfaces effectively destroy the homoge-

* Corresponding author. Fax: +1 510 486 5744.
E-mail address: elharel@berkeley.edu (E. Harel).

1090-7807/$ - see front matter Published by Elsevier Inc.
doi:10.1016/j.jmr.2008.04.037

neity at the site of the microfluidic device in a high-field magnet. While there may be ways to fabricate chips and coils to overcome this magnetic susceptibility problem they are generally incompatible with well-established protocols for chip fabrication already in place.

Detection off the chip allowed us to simultaneously image the flow of two fluids in a simple T-shaped chip as they converge into the outlet channel irrespective of the homogeneity of the magnetic field on the chip itself ([11]). However, the time resolution of the fluid flow is determined by the observation time of the spins inside the detection coil. For example, a readout time of 1 ms would result in ~1000 Hz spectral resolution, precluding any type of high-resolution NMR spectroscopy on or off the chip. There is no obvious way to avoid or circumvent this apparent uncertainty principle which is inherent in Fourier-related domains of the experiment owing to the Fourier uncertainty relation. It then appears that any type of spectrally resolved imaging, whether direct or remote, is fundamentally limited by this uncertainty relation.

For dynamic imaging, the state of the art in spectrally resolved MRI (e.g. EPSI) can achieve no better than ~ 20–50 ms time resolution at optimal conditions ([12]). On a microfluidic chip it is unlikely that the sensitivity of direct detection and the extremely fast flow rates of the fluids could ever allow such imaging sequences to be used which rely on relatively high sensitivity and homogeneity. Here, we show that the Fourier uncertainty condition can be significantly relaxed in the case of flow because space and time are related by velocity. This means that by partitioning space, one can effectively partition time if the velocity is constant in the detector. The former, in MRI, is accomplished simply by imaging along the flow direction. Using this principle, we demonstrate a time resolution an order of magnitude better than achieved without time slicing, about 2 ms. This is, in fact, the highest frame rate ever recorded for MRI. We believe that with simple improvement in hardware and pulse sequence design we can achieve a time resolution better than 100 μs, a regime which would allow fast dynamics previously inaccessible to NMR to be studied inside microfluidic devices for a wide range of problems. This would allow, for example, the characterization of fast mixing at any point inside the microfluidic device under continuous flow mode. Another powerful application would be in on-chip chromatography in which compounds present in a mobile phase would be separated in time by an interaction with a stationary phase present in the channels of the microfluidic device. Not only could the time of arrival of the analytes be measured with high time resolution by their unique NMR signature but also the location of the separation could be imaged.

2. Experimental details

The experimental setup, shown in Fig. 1, consists of two probes positioned head to head inside the bore of a superconducting magnet (Oxford, 7.0 T). The encoding coil (Varian Inc., Palo Alto, CA) used to excite the spins is placed from below the magnet, while the homebuilt detection probe is placed from above. This arrangement insures that both probes reside inside the homogeneous region of the magnetic field, while at the same time being situated in the linear part of the gradient stack (red coils in Fig. 1B). The two RF coils are shielded from one another

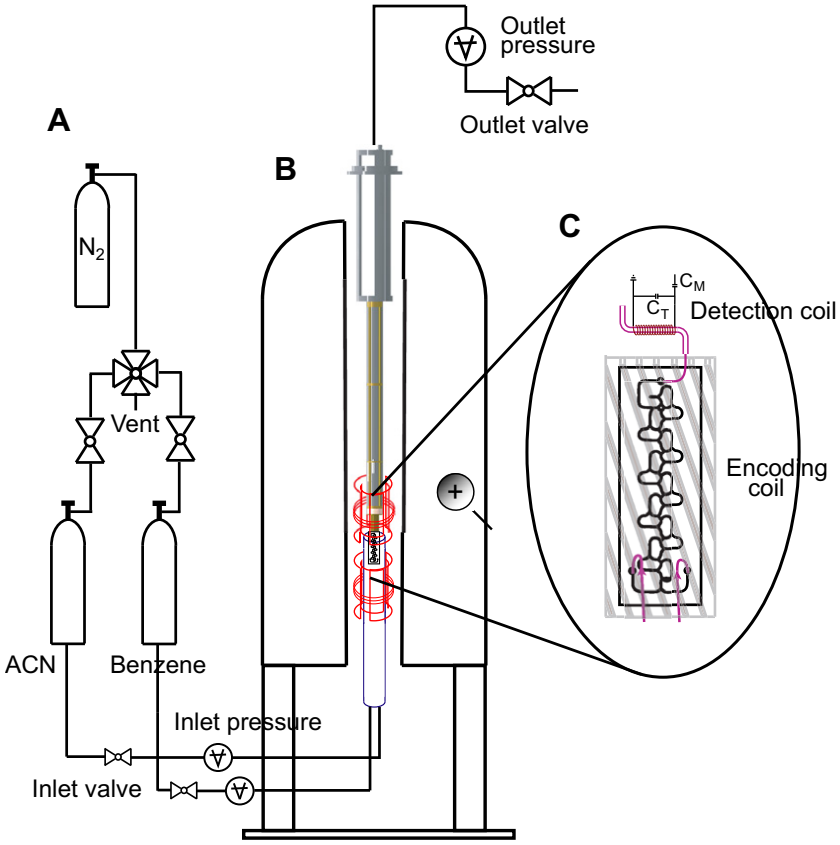

Fig. 1. Experimental setup. (A) Benzene and ACN are delivered to the microfluidic chip by pressure driven flow. (B) The chip, which resides inside the encoding coil, is situated approximately 1 cm below the shielded detection probe which is inserted from above the magnet bore. Both encoding and detection coils are encased by imaging gradients (coil pairs shown in red). (C) The fluid flows from the encoding coil to the outlet capillary with a 5 mm long, 1 mm ID detection coil wound around it. (For interpretation of the references to color in this figure legend, the reader is referred to the web version of this paper.)

by a copper hat which effectively eliminates unwanted excitation of spins inside the microfluidic chip during detection.

Pure ACN and benzene are pressurized with nitrogen gas at 50 psi and housed in stainless steel cylinders (Fig. 1A). The flow rate of each fluid is controlled by microvalves (Upchurch Scientific, Oak Harbor, WA) and monitored by employing an inversion recovery sequence in the detection coil, which effectively delays the time between an inversion pulse (180 degrees) and an excitation pulse (90 degrees) to measure the residence time of the mixed fluids in the detector. The microcoil was constructed out of 99.9% Cu wire with a polyimide coating wound around a 1 mm capillary (Fig. 1C). The capillary was then removed to allow PEEK tubing (Upchurch Scientific, Oak Harbor, WA) with a 360 μm OD and 150 μm ID to pass through. Variable capacitors (Johanson, Boonton, NJ) and chip capacitors (Voltronics corporation, Denville, NJ) completed the RF resonance circuit. Each probe was connected to independent RF amplifiers with the detection probe connected to the transmit/receive channel of the spectrometer (Varian, Inova). The encoding coil was controlled by the decoupler channel of the spectrometer which allowed for high precision pulse shaping. The 90-time of the encoding coil is approximately 120 μs at 52 dB of the maximum power, while the 90-time of the detection coil is 1.0 μs at the same amplifier power.

3. Methodology

3.1. Remote detection

The details of the remote detection methodology including a discussion of the sensitivity gains are described elsewhere ([13]). A remote detection experiment is like any other magnetic resonance experiment with a few notable exceptions. Encoding proceeds in the same manner as any other pulse sequence—spins are excited in some manner, either by spatial, spectral, or broadband selection, and then allowed to undergo some type of phase evolution. This evolution can be by means of the chemical-shift, scalar couplings, magnetic field gradients, etc... Typically, readout along the time axis is performed here as in the case of a conventional MR experiment. However, the detector is so insensitive that poor signal-to-noise precludes acquisition at this junction. The idea behind remote is to 'store' this phase information as longitudinal magnetization by application of a broadband pulse. The phase, ϕ, which contains the desired information is then transformed into $\cos\phi$. The transverse components of the magnetization decay in the limit that $T_1 \gg T_2$.

The price of storing the phase in this manner is that each data point that would conventionally be readout along one time course, must now be recorded point-by-point. In other words, $\Omega_1 t$, where $\Omega_1 t$ is either the internal or imposed frequency of the spin precession, must be read out as $cosi\Omega_1\Delta t$, where i goes from 0 to $t^{max}/\Delta t$. In the case of imaging, this translates to performing the experiment in a constant-time manner and arraying the gradient strengths as to cover the entire k-space trajectory. The stored phase, now directed along the axis of the static field, is relatively long lived (i.e. T_1), such that it can be flowed into a detector positioned downstream. The magnetization is then readout by a train of pulses which are spaced apart by the residence time of the fluid inside the detector.

The experiment is repeated until the entire Fourier space is recorded. Another way to think about this is that remote adds an additional experimental dimension to any conventional NMR or MRI experiment. For example, a one-dimensional spectrum becomes a two-dimensional experiment. A two-dimensional image is acquired by a two-dimensional pure phase encoding experiment. In conventional imaging, this type of experiment would yield the spectrum, but because the remote sequence eliminates the directly acquired time axis, the spectrum is lost and only the image is formed. The gain is that the readout can be performed in a highly sensitive, highly homogeneous environment. In short, a remote detection experiment is advantageous when the sensitivity in the vicinity of the sample is too poor for a direct acquisition.

3.2. Chemical-shift selection

For the case of fluid mixing, remote has an additional advantage over direct detection besides the previously mentioned sensitivity gain. If the two fluids to be imaged have distinct chemical-shift spectra, but the inhomogeneity in the detector is too poor to resolve them, it is still possible to differentiate the two species by remote detection. The reason is that the spectra are distinguishable in the detector if the residence time is sufficiently long to resolve each resonance. Since the species are assumed not to react, they maintain their chemical-shift signature throughout the course of the experiment. The detector is not in the vicinity of the sample so that it can be made to be highly homogeneous and free from type of susceptibility artifacts induced by the sample. For microfluidic applications, this unique feature is highly advantageous since the linewidths on the chip can exceed tens of kHz and completely preclude identification by the chemical-shift. Additionally, this type of differentiation does not come at any additional overhead in terms of experiment time. Each detection pulse yields a spectrum of the entire fluid mixture. Integrating each peak area then proceeds in the post-processing. Choosing one peak will result in reconstruction of an image of only that fluid species for which it belongs. This idea was demonstrated in a previous publication ([11]).

3.3. Time-of-flight

A feature of remote that was not immediately recognized when the method was first proposed was the ability to provide detailed flow information for imaging applications. During encoding, each voxel in the image is tagged by a phase as in a conventional MRI experiment. These encoded voxels then travel to the detector which pulses in intervals of the residence time. Therefore, for each voxel, a travel curve is recorded which gives information about the time-of-flight (TOF) as well as the dispersion owing to the spreading of the fluid packet due to no-slip conditions and other geometric constraints. A projection along this TOF axis yields the entire image. The effective time resolution is, therefore, given by the residence time of the detection coil. The smaller the ratios of volumes of the detection coil relative to the encoded volume, the higher the time resolution of the fluid flow. TOF imaging can, therefore, provide valuable information even when the sensitivity gain of a remote experiment is significant. For microfluidics, since the fluid must flow by definition, remote detection provides both a huge boost in sensitivity as well as providing valuable flow information. From this standpoint, the additional dimension of the remote experiment is not wasted, it provides for TOF information, which, otherwise, could not be measured. This global flow information compliments local flow measurements such as velocity encoding.

3.4. Ultrahigh time resolution

The ultrahigh time resolution scheme which is the focus of this work is shown in Fig. 2. As previously mentioned, the encoded spins flow into the detector which excites them back into the transverse plane where they continuously precess under the effects of the chemical shift and imposed magnetic field gradients. The duration of the encoded fluid in the detector is given by the residence time, T_R, which is chosen to be long enough to allow

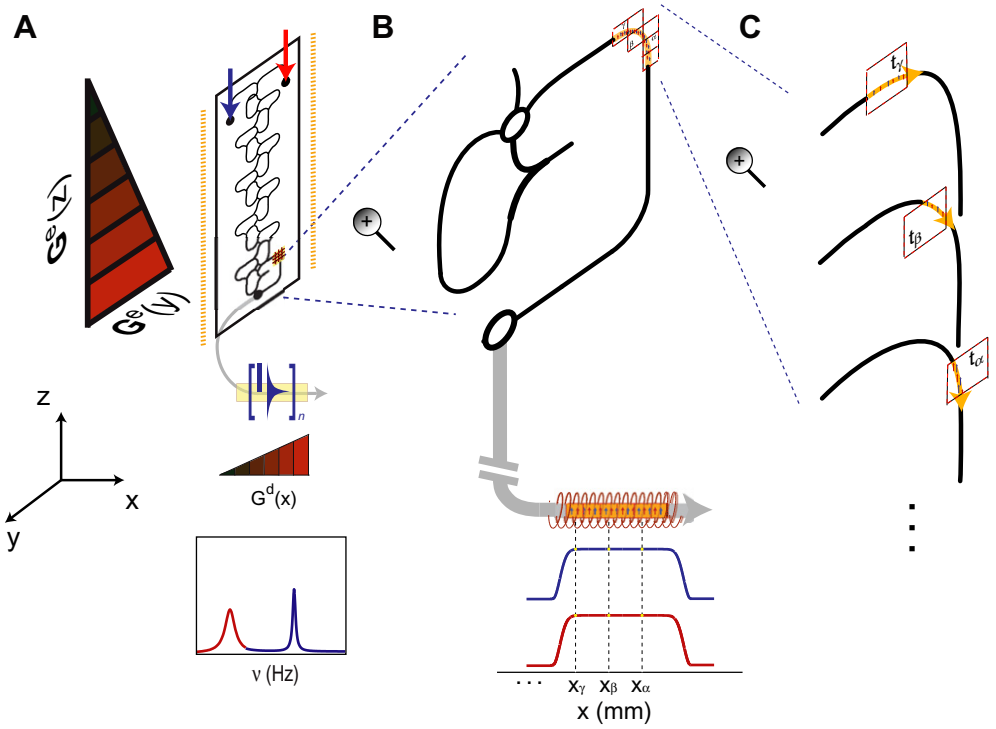

Fig. 2. Schematic of an ultrahigh time resolution remote detection TOF imaging experiment applied to a microfluidic chip.

the different species to be spectrally resolved. During acquisition, a 1D image is reconstructed by the application of a magnetic field gradient along the direction of flow, now along the x direction, which to a good approximation has a well-defined velocity, v_x. Imaging in the detector is accomplished by either phase encoding or by frequency encoding with a spectrally selective pulse. In either case, a 1D profile of the fluid inside the coil is measured for each fluid component.

To understand the way in which the time resolution is increased by means of adding an additional experimental dimension, consider the close-up of a region of the microfluidic chip showing a set of encoded voxels (orange squares in Fig. 2B). Each voxel contains either one or both of the fluid components (red and blue arrows) which are encoded according to the scheme described above. The earlier encoded voxel to arrive (labeled α) is nearer to the outlet. If this voxel is smaller than the detection volume it represents a section of the 1D profile along the detection coil axis. Some dispersion occurs so that this voxel may be spread over a larger volume than initially encoded (see Appendix). The spatial resolution along the detection coil axis therefore determines to what degree the initial voxel can be resolved in time. Fig. 2C shows a schematic of what each image constructed from a single point along the 1D profile would look like. Since the chemical species are assumed not to react, a spectrum of the mixture is recorded for each detection pulse as shown in Fig. 2A. By selecting a peak over which to integrate in the post processing of the data, an image is reconstructed for each chemical species. The spectral resolution of this spectrum is determined by T_R, the residence time in the detection coil and the separation between detection pulses during stroboscopic acquisition.

Fig. 3A shows the travel curve for all the spins in the microfluidic device, while 3B shows an FID following a single detection pulse. The spectral resolution is approximately, $1/T_R$, since T_R determines the effective relaxation time under conditions when $T_2 < T_R$, which is almost always the case in these type of microcoil experiments under continuous flow. If no image in the detector is

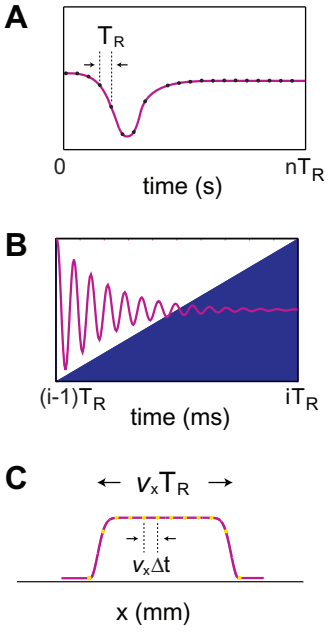

Fig. 3. (A) Travel curve all encoded spins. Each point is separated by T_R, the residence time in the detection coil. (B) An FID is recorded for the duration T_R following each detection pulse. In the ultrahigh time resolution modality, an image is recorded for each detection pulse for each chemical species. The spatial resolution, Δx, is related to the temporal resolution, Δt, through the proportionality factor, v_x which is the velocity of the fluid inside the detector.

recorded, the time resolution is given by T_R. However, if an image with a resolution of N pixels is recorded along the detector axis, the time slicing becomes approximately T_R/N. Since N is chosen independently of T_R, the spectral and time resolution are effectively decoupled. Notice that a higher time resolution could also be achieved simply by constructing a smaller coil at the same flow

velocity of length x_{coil}/N. However, the spectrum would then be broadened by a factor of N in accordance with the Fourier uncertainty. One could, of course, envision a scheme where the flow is stopped in this smaller detector momentarily to increase the spectral resolution and the spin packet moved with extreme control over the coil length for subsequent acquisitions. However, this would lead to significant relaxation and diffusion of encoded spins in queue to the detector and negate many of the advantages of remote detection. In effect, by imaging in the detector the effective time resolution is given by the product of the reciprocal velocity in the detector and the spatial resolution. By controlling the image resolution through the use of gradients the time resolution appropriate for the experiment, taking into account the flow velocity and available sensitivity, can be readily adjusted.

4. Results and discussion

4.1. Reconstructing TOF images with remote detection

The initial excitation pulse on the encoding channel consists of either a hard pulse to excite all the spins on the chip or a spatially selective pulse, typically a *sinc* in the presence of a pulsed gradient. The pulse sequence is shown in Fig. 4 for the case of pure phase encoding along the detector dimension. The gradients along y and z are used to reconstruct the imaging information of the face of the microfluidic device while the gradient along x is utilized for imaging the detector for increasing the time resolution of the experiment as described below.

After initial excitation with a 90 degree pulse the spins evolve under the presence of gradients along directions parallel to the face of the chip for a period of time between 50 and 100 μs. The gradient strengths used here did not exceeded 10 G/cm, while the maximum strength of the microimaging gradient stack is 100 G/cm along each direction. However, at very short gradient evolution times, coil rise times become the limiting factor in reducing the total encoding time (~1 μs per 1 G/cm). After evolution, the magnetization is stored along the longitudinal axis by the application of a hard pulse which acts across the entire sample. The phase of this pulse is arrayed in steps of 90 degrees for phase cycling, which is necessary to remove the baseline signal due to unencoded spins as well as to obtain frequency discrimination. The receiver phase was set to match that of the storage pulse.

The magnetization, having been stored along the longitudinal direction, now flows to the detector where it is read out by a series of hard, 90 degree excitation pulses. Storage of the spin magnetization is necessary when the transverse relaxation time is shorter than the flow time to the detector. Under most circumstances this is the case. The spins are now only subject to T_1 relaxation which is typically much longer than the effective transverse relation time, T_2^*. In order to obtain imaging information, the magnetization is allowed to precess in the presence of a gradient now directed along the coil axis (set to the x direction).

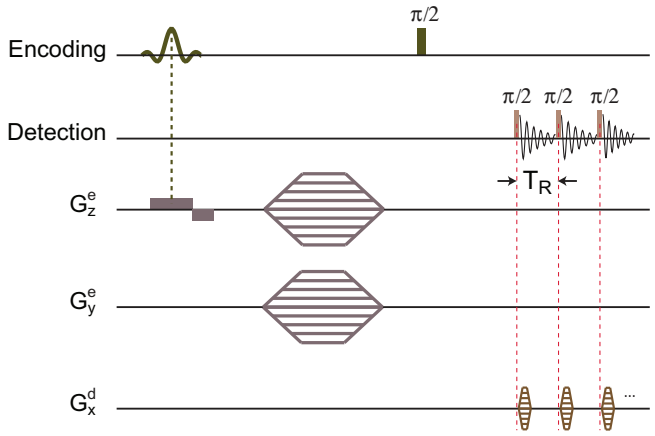

Fig. 4. Remote detection pulse sequence with ultrahigh time resolution. G_z^e and G_y^e are used to reconstruct partial images (i.e. constant-TOF images) of the face of the microfluidic chip, while G_x^d is used for converting between the detector imaging dimension and the increased TOF temporal resolution.

4.2. Spectral discrimination outside the sample

Spectral information is retained in one of two ways as described shortly. Because no reaction or transfer of spin coherence is assumed to take place in the detector one can correlate the imaging information with the chemical shift information in the detector only. The residence time was measured by an inversion recovery experiment to be about 20 ms, which, according to the uncertainty principle is enough time to separate resonance that are more than 50 Hz apart, which is adequate to clearly distinguish the single ACN and benzene resonances. Imaging in the detector was performed in two ways: one was a pure phase encoding sequence in which the experiment was repeated, each time with a different gradient strength along the coil direction but for a constant period of time. The integrated data set was then Fourier transformed to obtain a 1-D profile along the coil axis. Because the phase encoding is very short (<50 μs) the vast majority of the time the spins reside in the detector is left for chemical shift evolution of the spins which allows the spectra to be resolved. While this method adds an additional indirect dimension, it is the most robust. Furthermore, it provides the entire spectrum without additional overhead so that each fluid component is simultaneously imaged. In cases where more resolvable fluid components than time points are required, this method scales preferentially. The experiment can also be performed with spectrally selective pulses which excites each resonance in the detector followed by a spin echo frequency encoding pulse sequence. This provided higher time resolution (<1 ms) but suffered signal loss due to the difficulty of accurate spectral selection during fast flow and poor spin refocusing. However, this method required the least experiment time since no additional indirect dimension was necessary as with the phase encoding scheme. For cases in which only a few components are to be analyzed this method is immediately scalable.

4.3. Comparison with direct detection

The total experiment time for the pure phase encoding scheme just described is given by the total flow time through the chip multiplied by the number of indirect points multiplied by the number of phase cycles. For the data shown, the flow time is approximately 1.0 s and the number of points is given by the resolution along all three gradient axes $(15 \times 61 \times 11 = 10065)$. This results in an approximately 11 h acquisition time. For the frequency encoding scheme the experiment time is reduced by a factor of 11 since no phase encoding is necessary in the detection coil. However, a different experiment must be run for each fluid species, reducing the gain by a factor of two. The total experiment time for this scheme is approximately 2 h. The fast flow rate, however, makes frequency encoding less robust and provides inferior SNR. The number of partial images obtained with the pure phase encoding scheme is given by the number of detection pulses times the number of points taken in the detection coil dimension. This equals 1100 partial images. Therefore, while the total acquisition is relatively long each image, on average, takes only 36 s. This is in contrast to the long time needed to obtain a single image (albeit at slightly higher spatial resolution) directly under stopped flow conditions.

Fig. 5A shows a high-resolution direct image of water inside the microfluidic chip used in these studies. The fluid was stationary

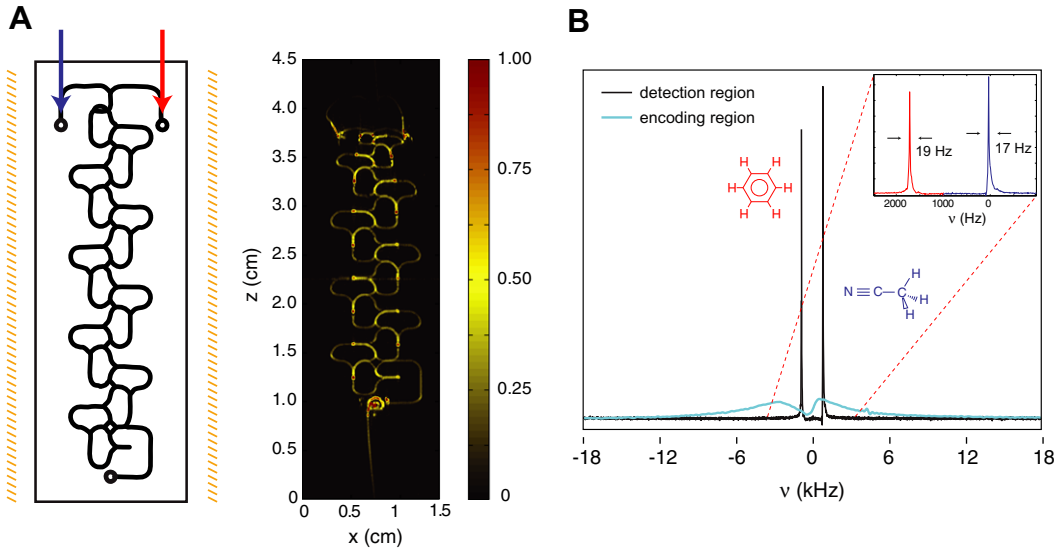

Fig. 5. Chemically resolved remote detection MRI. (A) Direct spin echo image. (B) High resolution spectra in each coil during stopped flow condition with benzene and ACN.

during the image acquisition since under flow no image was obtainable. This spin-echo sequence refocuses inhomogeneities and requires a 10-h scan time for 128×128 pixels along a 1.5 cm $\times$ 4.5 cm field-of-view (FOV) of the face of the 3 D mixing chip. In contrast consider the results of imaging by remote detection. Benzene and ACN were separated by their chemical shifts in the detection region as shown in Fig. 5B. The resolution in the 5 mm long coil is high relative to the encoding region where susceptibility broadening destroys most of the signal, clearly illustrating the advantages of remote detection. The spectrum recorded from the chip comes from a 1 cm slice through the center of the chip. Its width exceeds 6 kHz for a volume of about 4 μL. The ratio of detectable volume in the encoding coil to the detection volume is less than 10^{-4} for each component. The detection volume is approximately 100 nL but with a homogeneity better than 0.1 ppm (<20 Hz, proton; see inset of Fig. 5B). The ratio of detectable volume in the detection coil to the detection volume is approximately 2%.

4.4. TOF imaging of 3D mixing chip

Fig. 6 shows remotely detected TOF images acquired by pulsing the detection coil every T_R without the application of an imaging gradient in the detection dimension. Each panel represents the spatial locations of spins that took a given amount of time to reach the detector—that is, an isosurface of constant time-of-flight (TOF). The progression through the chip can be seen with the last panels corresponding to the inlet where each fluid species enters. The spatial resolution was set to 15×61 (30×122 after zero-filling), which was sufficient to resolve the structural features of the chip. At 500 ms TOF, the fluids mix showing the effectiveness of the mixing geometry of this microfluidic chip. At 580 ms TOF, the inlet for each respective fluid species can be seen (benzene top panels, ACN bottom panels), indicating that the mixing time is less than 80 ms.

In order to obtain the ultrahigh time resolution, an image is reconstructed for each detection pulse. The encoded fluid packet arrives, on average, every T_R to the detector. It is this time that defines the observation period of the measurement. Because $\Delta\nu < T_R^{-1}$, the fluids can be separated by their chemical-shift. The TOF resolution, however, can be sliced by imaging along the flow dimension, so that instead of being given by T_R, it is now given by T_R/N, where N is the number of points in the 1D image. N can be chosen arbitrarily up to the detection limit or hardware limitations. In order to obtain both the image and the chemical shift, a spectroscopic image in the detector is needed. This can be achieved in several ways by adding an indirect dimension to the experiment as previously discussed.

Fig. 5 shows a small subsection of the images obtained from the full integrated data set. Many interesting features of the flow can be seen at the 4 ms timescale displayed that are not apparent without the time slicing (although 2 ms resolution was obtained no significant changes are seen on this fast time scale at this spatial resolution). This subsection of the data shows two regions, one very close to the outlet and one slightly further away (later TOFs correspond to spins further from the outlet and detector). The region closest to the outlet region of the chip shows the effects of the higher time resolution more apparently since in this region dispersion is minimized, i.e. the spins have had less time to undergo Taylor dispersion. Due to the geometry of the chip there is significant dispersion created by the 3D mixing channels which act to stretch the fluid for improved mixing.

The similarity of the images of the ACN and benzene shows that the fluids are fairly well mixed at the outlet; however subtle differences still appear. For example, while the flow in the channels appears nearly identical indicating good mixing, the TOF patterns appear slightly different at the outlet connector which couples the chip to the external capillary tubing (green curve of Fig. 7B). This indicates that the fluids may begin to separate in this region. However, the lineshapes of the spectrum in the detector indicates that the fluid remix by the time they reach the detector. Each dispersion curve provides quantitative information for each chemical species at any point on the chip.

The TOF dimension replaces the direct dimension normally reserved for readout in direct MR experiments. This allows the dispersion curves for each voxel from the spatial dimensions of the chip to be recorded, providing a large amount of information about the flow properties of the various fluids ([14]). When one considers the number of 2D time-resolved images obtained in whole, the total acquisition time per frame is rather fast (<36 s for pure phase encoding and <7 s for frequency encoding, in comparison to the 10 h acquisition necessary to obtain the single image shown in Fig. 4A with direct detection and stopped flow). Even if, somehow, a direct experiment could be devised that would allow such fast acquisitions,

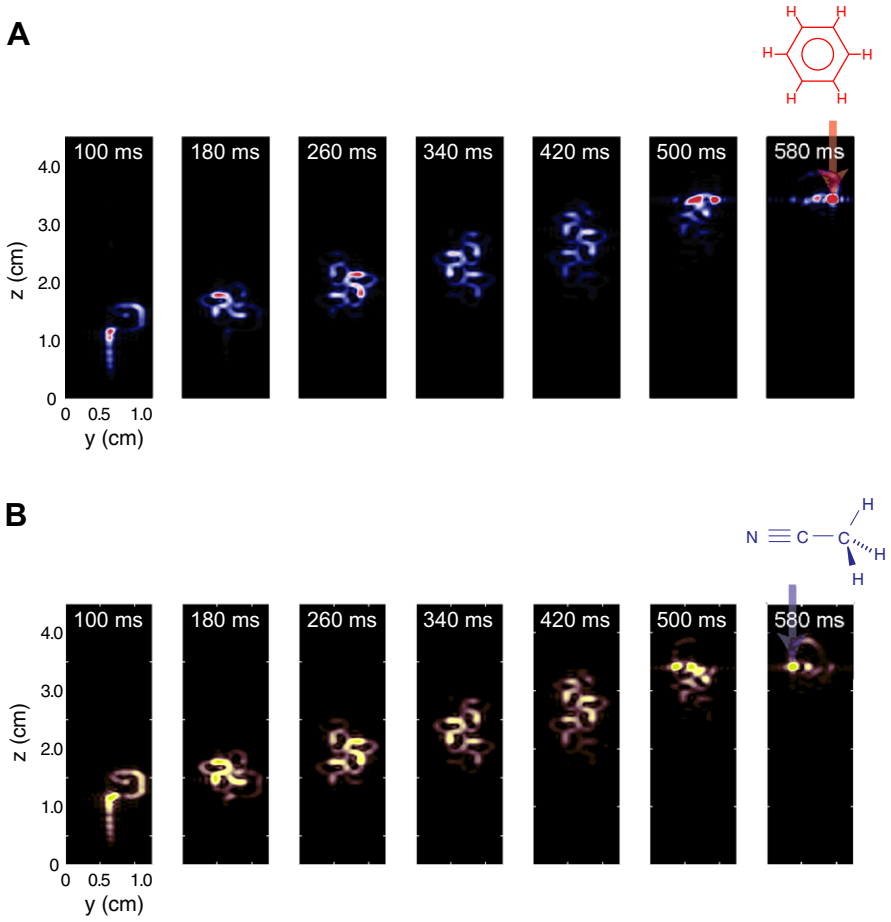

Fig. 6. Chemically resolved remote detection MRI. (A) Direct spin echo image. (B) High resolution spectra in each coil during stopped flow condition with benzene and ACN. (C) Remote detection partial images separated by T_R.

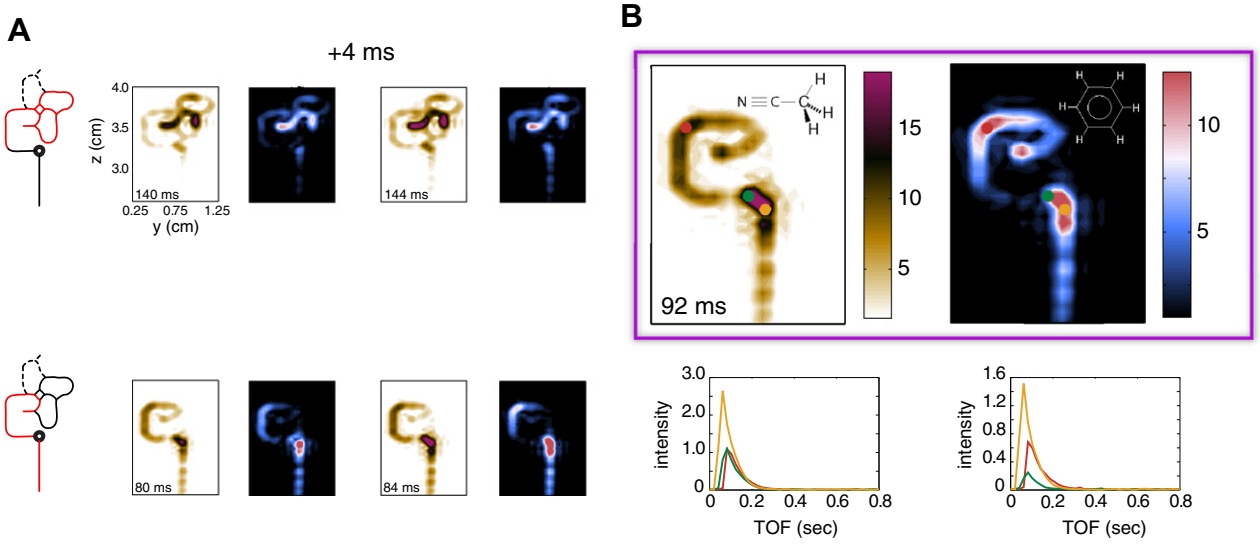

Fig. 7. Ultrahigh time resolution flow imaging. (A) TOF images of each fluid species at select times from the large integrated data set. (B) Zoomed in region of one of the TOF panels at 92 ms. For each voxel (red, orange, and green) in the image a TOF travel curves is available which provides more quantitative flow and dispersion information. (For interpretation of color mentioned in this figure the reader is referred to the web version of the article.)

the sensitivity of any coil surrounding a large, macroscopic chip is so weak as to make any attempt prohibitively difficult. It is therefore highly advantageous that such an experiment be done remotely.

5. Conclusion

We have demonstrated a method for spectrally-resolved ultra-high time resolution MRI that is not limited by the Fourier uncer-

tainty criteria. The information rich content of the integrated data set accompanying this experiment allows for a detailed analysis of the fluid and chip properties, even when the flow is irregular or pulsatile, provided the phase of the pulsation is known. Many methods for increasing the sensitivity exist. Here the filling factor was approximately 2% while others have shown the possibility of microsolenoid coils with filling factors of 70% or greater by using thinner walled tubbing. Furthermore, the homogeneity in this experiment was only 0.1 ppm in the detector while others have reported better than 0.01 ppm with the aid of susceptibility matching fluids. Taking advantage of both a filling factor improvement, matched encoded fluid and detection volumes, and stopped or slowed flow detection could increase the sensitivity by at least two orders of magnitude. Concentrations in the millimolar range are routinely detected with microsolenoid NMR probes making the detection of the dynamics of biological samples in microfluidic devices possible with this method ([15,16]).

Improvements in pulse sequences and the incorporation of more sophisticated microfluidic components could significantly speed the experiment acquisition time in many instances, for example, when collecting information over a small sub-volume of the chip. Because the fluid residence time through a small sub-volume is only a fraction of the residence time through the entire device the experiment can have a much shorter recycle delay. This would allow zooming in any region of interest with high spatial and temporal resolution on microfluidic devices of arbitrary complexity, an accomplishment not foreseeable with direct detection MRI means even with the use of surface coils fabricated as part of the chip. No modifications of the chips are necessary here and no specialized coils or hardware on the chip itself are required. The use of an auxiliary detection probe ([17]) makes the technique versatile and compatible with current NMR microimaging systems. The addition of plugged flow has the potential to localize the dynamics of single encoded voxels with volumes below 1 nL. Future applications will focus on applying this method to protein ligand binding dynamics by way of on-chip chromatography at an ultrahigh time resolution previously inaccessible to NMR.

Acknowledgments

We thank Tyler Meldrum for helpful discussions, and Louis Bouchard, Vik Bajaj, and Professor David Wemmer for critical reading and most helpful suggestions on the manuscript. This work is supported by the Director, Office of Science, Office of Basic Energy Sciences, and Materials Sciences Divisions of the U.S. Department of Energy under contract DE-AC03-76SF0098.

Appendix A. Dispersion Considerations

Quantifying the mechanics of the fluid flow through such a complex chip is extremely challenging and beyond the scope of this work. However, it is possible to estimate the dispersion of pressure-driven flows through the etched channels of the chip. The main mechanism for this effect is the no slip boundary condition at the walls of the microfluidic channels. For a given encoded voxel element of volume V_0 and length L_0, the spreading of the fluid due to Taylor dispersion can be estimated. Because the Peclet number in the direction of the motion is much greater than unity we can effectively ignore diffusion along this dimension. The ratio of the dispersion length to an initial voxel length is given by

$$\frac{L_D}{L_0} = \left[\frac{tQ^2d^2}{105DV_0^2} f\left(\frac{d}{W}\right)\right]^{1/2}$$

where t is effectively the time-of-flight (TOF) and Q is the flow rate ([18]). The function, f depends on the exact geometry of the channel. For $d = 150\ \mu m$ and $W = 225\ \mu m$, (note, that the d/W here is 0.66, while Dutta and Leighton assume 0.5), the volume of one voxel is approximately 2.5 nL. This means that to a rough approximation the dispersion ratio is 5 for a TOF of 1 ms, calculated for pure water. Of course, this is not completely accurate since the channel profile does not have the exact shape described by Dutta and Leighton. Furthermore, the 3D mixing geometry most certainly affects the dispersion in a non-trivial manner. But we expect this estimate to be fairly accurate due to the highly laminar flow (very low Reynold's number) predicted inside the microchannels. The result of this rough calculation means that considerable time partitioning must be realized to get accurate localization of a single voxel at this spatial resolution. If the above formulation is correct, this would require a time resolution of roughly 40 μs. However, there are many methods to decrease or even nearly eliminate dispersion mechanically such as using plugged flow ([19]) or by profiling the cross sectional shape of the channel. Also it is possible to use a polymeric stationary phase anchored to the wall of the microchannel to create a slip boundary condition and, hence, minimize dispersion. Alternatively, it is possible to drive the flow by electro-osmosis which gives nearly uniform velocity profiles although the slow flow rates associated with this method make it less attractive for the remote detection NMR method described here.

References

[1] P. Von Lode, Point-of-care immunotesting: approaching the analytical performance of central laboratory methods, Clin. Biochem. 38 (2005) 591.
[2] S.J. Haswell, R.J. Middleton, B. O'Sullivan, V. Skelton, P. Watts, P. Styring, The applications of micro reactors to synthetic chemistry, Chem. Commun. 5 (2001) 391.
[3] J.W. Hong, V. Studer, G. Hang, W.F. Anderson, S.R.A. Quake, Nanoliter-scale nucleic acid processor with parallel architecture, Nat. Biotechnol. 22 (2004) 435.
[4] Y. Sato, G. Irisawa, K. Ishizuka, K. Hishida, M. Maeda, Visualization of convective mixing in microchannel by fluorescence imaging, Meas. Sci. Technol. 14 (2003) 114.
[5] R.H. Liu, M.A. Stremler, K.V. Sharp, M.G. Olsen, J.G. Santiago, R.J. Adrian, H. Aref, D.J. Beebe, Passive mixing in three-dimensional serpentine microchannel, J. Microelectromech. S9 (2000) 190.
[6] A.D. Stroock, S.K. Dertinger, A. Ajdari, I. Mezic, H.A. Stone, G.M. Whitesides, Chaotic mixer for microchannels, Science 295 (2002) 647.
[7] H. Rampel, J.M. Pope, Chemical shift imaging in nuclear magnetic resonance: a comparison of methods, Conc. Magn. Reson. 5 (1993) 43.
[8] K. Ehrmann, M. Gersbach, P. Pascoal, F. Vincent, C. Massin, D. Stamou, P.-A. Besse, H. Vogel, R.S. Popovic, Sample patterning of NMR surface microcoils, J. Magn. Reson. 178 (2006) 96.
[9] A.J. Moule, M.M. Spence, S.I. Hans, J.A. Seeley, K.L. Pierce, S. Saxena, A. Pines, Amplification of xenon NMR and MRI by remote detection, Proc. Natl. Acad. Sci. USA 100 (2003) 9122.
[10] J. Granwehr, E. Harel, S. Hans, S. Garcia, A. Pines, P.N. Sen, Y.Q. Song, Time-of-flight flow imaging using NMR remote detection, Phys. Rev. Lett. 95 (2005) 075503.
[11] E. Harel, C. Hilty, K. Koen, E.E. McDonnell, A. Pines, Time-of-flight flow imaging of two-component flow inside a microfluidic chip, Phys. Rev. Lett. 98 (2007) 017601.
[12] P. Mansfield, R. Turner, M.K. Stehling, Echo-planar imaging magnetic resonance imaging in a fraction of a second, Science 254 (1991) 43.
[13] J. Granwehr, J. Seeley, Sensitivity quantification of remote detection NMR and MRI, J. Magn. Reson. 179 (2006) 280.
[14] E. Harel, J. Granwehr, J.A. Seeley, A. Pines, Multiphase imaging of gas flow in a nanoporous material using remote detection NMR, Nat. Mat. 5 (2006) 321.
[15] D.L. Olson, T.L. Peck, A.G. Webb, R.L. Magin, J.V. Sweedler, High-resolution microcoil 1H NMR for mass-limited nanoliter-volume samples, Science 270 (1995) 1967.
[16] F.C. Schroeder, M. Gronquist, Extending the scope of NMR spectroscopy with microcoil probes, Angew. Chem. Int. Ed. 45 (2006) 7122.
[17] S.I. Han, J. Granwehr, S. Garcia, E.E. McDonnell, A. Pines, Auxillary probe design adaptable to existing probes for remote detection NMR, MRI, and time-of-flight tracing, J. Magn. Reson. 182 (2006) 260.
[18] D. Dutta, D.T. Leighton, Dispersion reduction in pressure-driven flow through microetched channels, Anal. Chem. 73 (2001) 504.
[19] R.A. Kautz, W.K. Goetzinger, B.L. Karger, High-throughput microcoil NMR of compound libraries using zero-dispersion segmented flow analysis, J. Comb. Chem. 7 (2005) 14.